Contact resistivity reduction through interfacial layer doping in metal-interfacial layer-semiconductor contacts

Shashank Gupta,[1] Prashanth Paramahans Manik,[2] Ravi Kesh Mishra,[2] Aneesh Nainani,[1] Mathew C. Abraham,[1] and Saurabh Lodha[2]
[1]*Applied Materials, Inc., Santa Clara, California 94085, USA*
[2]*Center of Excellence in Nanoelectronics, Department of Electrical Engineering, Indian Institute of Technology Bombay, Mumbai 400076, India*

(Received 17 March 2013; accepted 31 May 2013; published online 18 June 2013)

Metal-induced-gap-states model for Fermi-level pinning in metal-semiconductor contacts has been extended to metal-interfacial layer (IL)-semiconductor (MIS) contacts using a physics-based approach. Contact resistivity simulations evaluating various ILs on n-Ge indicate the possibility of forming low resistance contacts using TiO_2, ZnO, and Sn-doped In_2O_3 (ITO) layers. Doping of the IL is proposed as an additional knob for lowering MIS contact resistance. This is demonstrated through simulations and experimentally verified with circular-transfer length method and diode measurements on Ti/n^+-ZnO/n-Ge and Ti/ITO/n-Ge MIS contacts. © *2013 AIP Publishing LLC*. [http://dx.doi.org/10.1063/1.4811340]

I. INTRODUCTION

Logic technology device scaling requires aggressive reduction of the source/drain (S/D) contact resistivity to overcome contact area reduction resulting from dimensional scaling of the contact and S/D regions as well as introduction of new materials such as Ge and Si:C.[1,2] Fermi-level (FL) pinning near the valence band (VB) and low n-type dopant activation lead to a large (~0.55 V) and wide potential barrier for metal contacts on n-Ge resulting in high contact resistance.[3,4] Increased n-type dopant activation using co-implantation of P and Sb[5] or enhancing the electric field in the Ge substrate using techniques such as a triple interface of Ti/Au/Ge[6] has been recently reported. At the same time, insertion of an interfacial layer (IL) between the metal and semiconductor S/D (MIS contact) has been shown to alleviate Fermi-level pinning by multiple research groups.[7–9] The alleviation of Fermi-level pinning, in general, has been attributed to the reduction of Metal-Induced-Gap-States (MIGS) in the semiconductor band gap due to the insertion of a thin IL.[3,10] The relative extent of unpinning of the FL depends on the intrinsic properties of the IL such as band gap and dielectric constant.[10] However, insertion of an IL between the metal and the semiconductor increases the tunneling resistance of the contact and may dominate the total contact resistance depending on the thickness of the IL and its band offset with respect to the semiconductor.[11] Thus, careful optimization of IL properties and its thickness is needed to realize low resistance MIS contacts.

In this work, we extend the MIGS model for metal-semiconductor (M-S) contacts[12,13] to MIS contacts using a simple physics-based approach to analyze dependencies of the contact resistivity on various IL parameters. We improve upon recent reports on a MIGS model for MIS contacts by (a) calculating the FL pinning factor $S\,(=d\Phi_{bn}/d\Phi_M)$, where Φ_{bn} is the barrier height and Φ_M is the metal work function, for a specific IL with thickness t instead of assuming a wide range of values of S (0-1),[11] (b) considering incomplete unpinning of the FL ($S<1$) by ultrathin IL (<1 nm) instead of complete screening of MIGS by the metal/IL dipole resulting in full depinning of the FL for thicker IL,[14] and, (c) considering the series capacitive division of charge between the MIGS in the IL and MIGS in the semiconductor thereby accounting for the differences in their material properties.[10] Further, we introduce doping of the IL as an additional process knob that can significantly reduce the specific contact resistivity (ρ_c) and hence provides further improvement for MIS contact technology. Specifically, we demonstrate the benefit of IL doping for lowering contact resistivity using ZnO and Sn-doped In_2O_3 (ITO) as ILs on n-Ge substrates through simulations as well as experiments. Though we have recently published experimental reports of contact resistivity reduction using ZnO as an IL,[9,15] additional experimental data for ZnO as well as ITO along with physics-based modeling and simulation of MIS contacts make this a more widely applicable and comprehensive study of MIS contacts with doped/conductive interfacial layers.

II. MIGS MODEL FOR MIS CONTACTS

The physics of Fermi-level pinning in metal-semiconductor contacts has been well explained by the MIGS model given by Monch[12] where MIGS calculation using a one dimensional (1D) band structure has been shown to predict similar Fermi-level pinning results as given by other, more complex models.[13,16,17] We have extended the same model to MIS contacts. In this model, we propose that the M-IL interface has MIGS (similar to a M-S interface described by Louie *et al.*[13]) and its density at the M-IL interface ($D_{MIGS0IL}$) is given by the equation

$$D_{MIGS0IL} = \frac{2}{\pi a^2 E_g}. \quad (1)$$

In the above equation, a is the lattice constant and E_g is the band gap of the IL. The MIGS density (D_{MIGS}) falls off exponentially into the IL with a decay length (δ_{IL}) given by[12]

$$\delta_{IL} = \frac{h^2}{2\pi m_0 a E_g}, \tag{2}$$

where m_0 is the free electron mass and h is the Planck's constant. The exponential decay of D_{MIGS} at a distance t away from the M-IL interface is then given by

$$D_{MIGS}(t) = D_{MIGS0IL} e^{-\frac{t}{\delta_{IL}}}. \tag{3}$$

The MIGS density at the IL-S interface ($D_{MIGS}(t)$) can hence be evaluated by substituting IL thickness for t in Eq. (3). This value depends on the band gap and the lattice constant of the IL layer as is evident from Eqs. (1) and (2). The higher the band gap and the lattice constant, the lower is the MIGS density at the IL-S interface and hence more effective the IL is in depinning the Fermi-level. Knowing the MIGS density at the IL-S interface, its decay in the semiconductor (here Ge) is still given by Eq. (3) but δ_{IL} should be replaced by the decay length of MIGS in the semiconductor (here δ_{Ge}). Fig. 1 shows the MIGS decay in Ge with and without the IL, consistent with experimental observations of reduced Fermi-level pinning due to the presence of an IL. It is clear that the IL can significantly reduce MIGS density in the semiconductor. The Fermi-level pinning factor S is then given by the following equation (in accordance with Monch[12]):

$$S = \left(1 + q^2 \frac{D_{MIGS}(t)(\delta_{Ge}\varepsilon_{IL} + t\varepsilon_{Ge})}{\varepsilon_0(\varepsilon_{IL} + \varepsilon_{Ge})}\right)^{-1}. \tag{4}$$

Here, q is electronic charge, ε_0 is vacuum permittivity, ε_{IL} is the relative permittivity of the IL, and ε_{Ge} is the relative permittivity of Ge. It should be noted that the pinning factor (S) given by Eq. (4) takes into account the series capacitive division of charge between the IL of thickness t and the semiconductor with a decay length of δ_{Ge}. With this S value and the charge neutrality level (Φ_{CNLS}) near VB in Ge, the effective metal work function, Φ_{Meff}, can be calculated using

$$\Phi_{Meff} = S\Phi_M + (1 - S)\Phi_{CNLS}. \tag{5}$$

The above set of equations can be used to evaluate the pinning factor S and Φ_{Meff} as a function of IL thickness t for a given semiconductor (here Ge). The Φ_{Meff} can be used to construct equilibrium electrostatics for a given MIS contact. However, the total contact resistance depends on the tunneling resistance of the MIS stack. To evaluate the contact resistance, simulations were performed using the device simulator in the Synopsys TCAD framework employing a Wentzel-Kramers-Brillouin (WKB) non-local tunneling model. These simulations used the Φ_{Meff} values given by Eq. (5) in the model for a given IL thickness and therefore the contact resistance obtained incorporates both the reduction of Fermi-level pinning and increment of tunneling resistance with increasing IL thickness. This combination of a physics-based model and simulation helps in evaluating the ρ_c of a MIS contact for a specific IL with thickness t in a straightforward manner.

While the above formalism is based on the MIGS originating at the metal-IL (MI) interface and their effect on the electrostatics of the MIS contact, the difference in charge neutrality levels at the IL-semiconductor (IS) interface also gives rise to a dipole which needs to be accounted for in the electrostatics and resistivity calculations of the MIS contact.[14] Specifically, the IS dipole affects the potential barrier (Φ_{bn}) at the IS interface

$$\Phi_{bn} = \Phi_S - \chi_S - \Psi_S. \tag{6}$$

Here, Φ_S is the work function of the semiconductor, χ_S is its electron affinity, and Ψ_S is the total equilibrium band bending in the semiconductor (Fig. 1). Ψ_S depends on the IS dipole through the equation[14]

$$\Psi_S = -\frac{C_I}{C_I + C_S}\Phi_{MS} - \frac{C_{il}}{C_{il} + C_{iS}}\Delta_{IS}, \tag{7}$$

where Φ_{MS} is the difference between the metal and semiconductor work functions and Δ_{IS} is the insulator-semiconductor dipole voltage. C_I and C_S are the IL and semiconductor

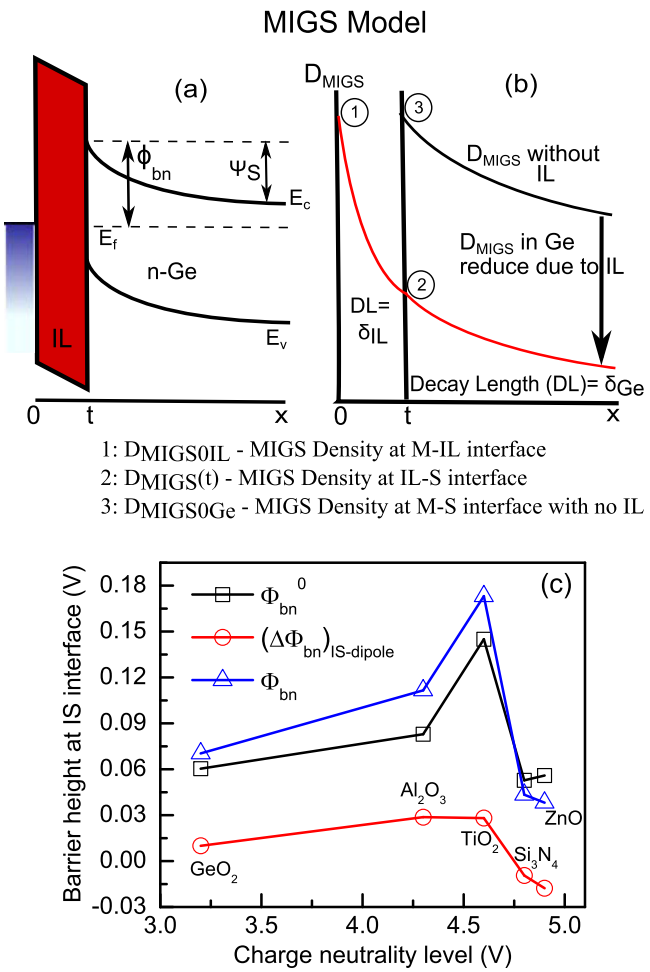

FIG. 1. MIGS model for MIS contacts showing (a) a simplified energy band-diagram, (b) density of MIGS (D_{MIGS}) decay in Ge with and without an IL, and (c) barrier height with (Φ_{bn}) and without (Φ_{bn}^0) the correction ($(\Delta\Phi_{bn})_{IS-dipole}$) due to the IS dipole at the IS interface for various ILs.

surface capacitance densities, respectively. C_{il} and C_{iS} are the IL-semiconductor dipole capacitance densities for the IL and the semiconductor, respectively. These capacitance densities and Δ_{IS} are given by[14]

$$C_I = \frac{\varepsilon_{IL}\varepsilon_0}{t}; \quad C_{il} = \frac{\varepsilon_{\infty IR}\varepsilon_0}{d_{il}}; \quad C_{iS} = \frac{\varepsilon_{\infty SR}\varepsilon_0}{d_{iS}}, \tag{8}$$

$$C_S(\Psi_S) = q\sqrt{\frac{\varepsilon_{Ge}\varepsilon_0 N_D}{2k_BT}} \times \left| \frac{e^{\frac{q\Psi_S}{k_BT}} - 1 - \left(\frac{n_i}{N_d}\right)^2 e^{-\frac{q\Psi_S}{k_BT}}}{\sqrt{e^{\frac{q\Psi_S}{k_BT}} - \frac{q\Psi_S}{k_BT} - 1 + \left(\frac{n_i}{N_d}\right)^2 \left[e^{-\frac{q\Psi_S}{k_BT}} - 1\right]}} \right|, \tag{9}$$

$$\Delta_{IS} = (1 - S_{IS})(\Phi_{CNLS} - \Phi_{CNLI}). \tag{10}$$

In the above relations, $\varepsilon_{\infty IR}$ ($\varepsilon_{\infty SR}$) and d_{il} (d_{iS}) are the high-frequency relative dielectric constant and dipole layer thickness, respectively, for the IL (semiconductor). N_D is the donor doping concentration, k_B is Boltzmann constant, T is temperature, and n_i is the intrinsic carrier concentration for the semiconductor. Φ_{CNLI} is the charge neutrality level of the IL and S_{IS} is the slope/pinning parameter of the IS interface.[14] The above methodology has been described in detail by Wager and Robertson.[14] In the current work, for a heavily doped n-type Ge substrate

$$\begin{aligned}\Phi_{bn} &= \Phi_S - \chi_S - \Psi_S \approx -\Psi_S \\ &= \frac{C_I}{C_I + C_S}\Phi_{MS} + \frac{C_{il}}{C_{il} + C_{iS}}\Delta_{IS} \\ &= \Phi^0_{bn} + (\Delta\Phi_{bn})_{IS-dipole}.\end{aligned} \tag{11}$$

In the above equation,

$$(\Delta\Phi_{bn})_{IS-dipole} = \frac{C_{il}}{C_{il} + C_{iS}}\Delta_{IS}, \quad \text{and,} \qquad \Phi^0_{bn} = \frac{C_I}{C_I + C_S}\Phi_{MS}. \tag{12}$$

The effect of the IS dipole can be considered as a correction $(\Delta\Phi_{bn})_{IS-dipole}$ to the ideal barrier height (Φ^0_{bn}) to get the actual barrier height (Φ_{bn}). Table I lists the key parameters used to calculate $(\Delta\Phi_{bn})_{IS-dipole}$ and Φ^0_{bn} for various ILs. Fig. 1(c) shows the values of Φ_{bn}, Φ^0_{bn}, and $(\Delta\Phi_{bn})_{IS-dipole}$ calculated for various ILs by self-consistently solving Eqs. (7) and (9) for Ψ_S using a value of 0.3 V for Φ_{MS}. It can be seen that the effect of the IS dipole on the ideal potential barrier at the IS interface (Φ^0_{bn}) is small.[14] In addition, Φ_{bn} is only a part of the total tunneling resistance besides the IL itself. Further, Fig. 1(c) suggests that the trend in Φ^0_{bn} for various ILs will not change if the correction due to the IS dipole is included. The above arguments suggest that the contribution of the IS dipole to the overall contact resistivity and its trend across various ILs can be considered insignificant. It is interesting to note that the large difference in the high (80) and low (7.8) frequency relative dielectric constants in case of TiO_2 leads to a large difference in the Φ^0_{bn} and $(\Delta\Phi_{bn})_{IS-dipole}$ values. Also, the magnitude of the correction term is negative in case of ZnO and Si_3N_4. This is because of net electron transfer from Ge to the ILs due to a charge neutrality level below that of Ge (4.7 V). In addition to MIGS, recent work[23] reports the effect of a net dipole arising from a difference in O-ion densities at the metal/IL and IL/semiconductor interfaces which requires the IL to act as a good diffusion barrier to oxygen. Such a dipole may aid MIGS in lowering the contact resistivity and needs to be considered in future extensions of the MIGS model for MIS contacts.

TABLE I. Key parameters used to calculate Φ^0_{bn} and $(\Delta\Phi_{bn})_{IS-dipole}$. $\Phi_{CNLS} = 4.7$ V, $N_D = 2.5 \times 10^{19}$ cm^{-3}, $d_{iS} = 0.4$ nm, $\varepsilon_{Ge} = 16$, and $\varepsilon_{\infty SR} = 16$ have been used for Ge.[14] $d_{il} = 0.4$ nm and $t = 1$ nm have been used for all ILs.

IL	$\varepsilon_{\infty IR}$	ε_{IL}	S_{IS}	Φ_{CNLI} (V)	Δ_{IS} (V)
Al_2O_3	3.4 (Ref. 18)	9	0.59	4.3 (Ref. 18)	0.16
GeO_2	1.8 (Ref. 10)	5.9	0.93	3.2 (Ref. 19)	0.10
Si_3N_4	3.8 (Ref. 14)	7	0.51	4.8 (Ref. 14)	−0.05
TiO_2	7.8 (Ref. 10)	80	0.14	4.6 (Ref. 20)	0.09
ZnO	3.7 (Ref. 21)	9	0.53	4.9 (Ref. 22)	−0.09

III. APPLICATION OF MIGS MODEL AND EFFECT OF IL DOPING

The model and the simulation methodology discussed in Sec. II were used to evaluate different ILs for relative effectiveness in reducing ρ_c. Relevant simulation parameters for various ILs are given in Table II. n-Ge was chosen as the substrate because of its technological relevance for device scaling and strong Fermi-level pinning near VB. Fig. 2 shows S for different ILs with varying thickness. ILs with larger E_g and higher lattice and dielectric constants are faster in unpinning the FL than others, as expected from the model described earlier. The IL thickness required to completely unpin the FL ($S = 1$) is proportional to δ_{IL} which makes it an important parameter in the design of MIS contacts. For example, approximately 3 Å (three to four times of δ_{IL}) of Al_2O_3 is needed to unpin the Fermi level, consistent with reported values.[24] It is important to note that the S in Fig. 2 is the effective value of the slope parameter for the combined metal/IL/Ge contact for various materials acting as the IL, and hence shows a dependence on IL thickness.[10] It is

TABLE II. IL simulation parameters (E_g, ε_{IL}, a, and m^* are the band gap, dielectric constant, lattice constant, and electron tunneling mass for the IL, respectively. $\Delta E_c(Ge)$ is the conduction band offset of IL with respect to Ge).

IL	E_g (eV)	a (Å)	ε_{IL}	m^*	ΔE_c(Ge) (eV)
Al_2O_3	8.8	4.785	9	0.2	2.8
GeO_2	4.3	4.402	5.9	0.7	0.6
Si_3N_4	5.3	7.608	7	0.2	1.9
TiO_2	3.05	4.593	80	0.3	−0.06
ZnO	3.37	3.249	9	0.3	−0.1
ITO	4.06	10.21	9	0.3	−0.1

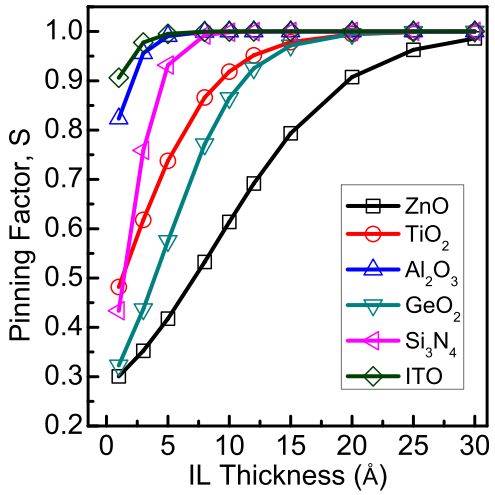

FIG. 2. Fermi-level pinning factor (S) for different ILs as a function of IL thickness.

different from the intrinsic pinning factor, S_{IL}, of the IL material itself, given by[12]

$$S_{IL} = \left(1 + q^2 \frac{D_{MIGS0IL}\delta_{IL}}{\varepsilon_0 \varepsilon_{IL}}\right)^{-1}. \quad (13)$$

Using the above equation along with Eqs. (3) and (4), the effective S for the MIS contact can be rewritten in terms of S_{IL} as follows:

$$S = \left(1 + \frac{\varepsilon_{IL}(1 - S_{IL})e^{-\frac{t}{\delta_{IL}}}(\delta_{Ge}\varepsilon_{IL} + t\varepsilon_{Ge})}{S_{IL}\delta_{IL}(\varepsilon_{IL} + \varepsilon_{Ge})}\right)^{-1}. \quad (14)$$

The overall ρ_c of MIS contacts depends not only on the unpinning of the FL but also on the tunneling resistance offered to electron conduction by the IL, which in turn depends on the conduction band offset of the IL with respect to the semiconductor (ΔE_c). Fig. 3 shows the ρ_c of MIS contacts for different ILs with varying thickness on n-Ge. An active doping concentration of 1×10^{19} cm^{-3} was chosen for the n-Ge layer, similar to experimental reports of maximum active concentration of P in Ge.[5] The contact resistivity simulations take into account both the unpinning of FL by different ILs and the series tunneling resistance added to MIS transport. ILs such as Al_2O_3, Si_3N_4, and GeO_2 show faster unpinning but add substantial tunneling resistance due to large ΔE_c. On the other hand, ILs such as TiO_2 and ZnO, though slower at unpinning, add minimal tunneling resistance due to small ΔE_c even for thick (~3 nm) layers and

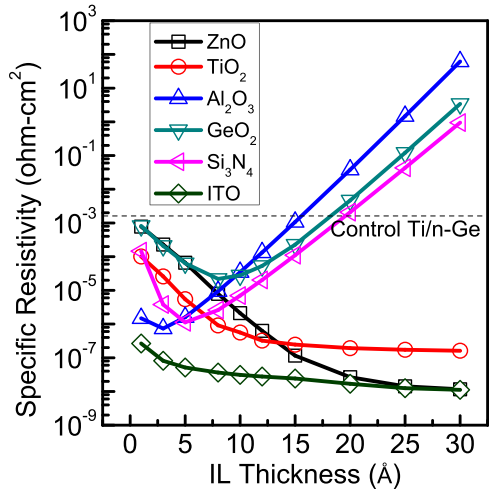

FIG. 3. Specific contact resistivity simulation results for different ILs as a function of IL thickness.

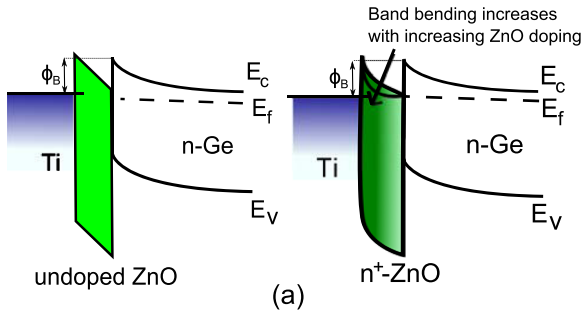

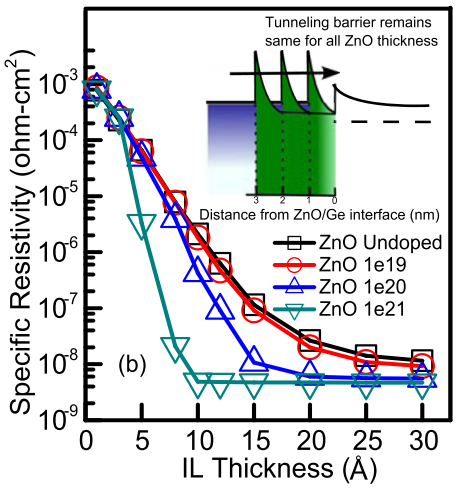

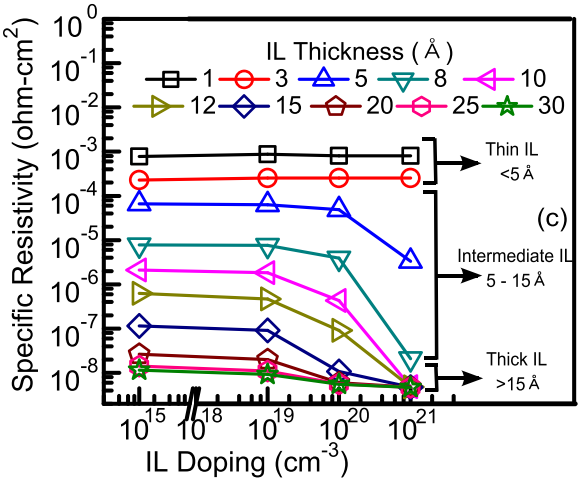

FIG. 4. (a) Schematic illustrating thinning of tunneling barrier due to IL (ZnO) doping, (b) specific contact resistivity simulation results of MIS contacts for varying ZnO (IL) thickness showing the insensitivity of contact resistivity to IL thickness for thicker ILs that increases with higher doping, and (c) specific contact resistivity for varying IL doping showing three different regimes of IL thicknesses for contact resistivity dependence on doping (depletion width).

hence are more viable. Finally, ITO unpins quickly due to its large lattice constant without significant increase in the contact resistance due to a small ΔE_c.

In addition, ZnO can be easily doped n-type by generating oxygen vacancies (Vo) that act as donors,[25] whereas Sn acts as a donor in ITO. Fig. 4(a) illustrates the effect of IL doping on MIS transport for the case of a ZnO IL. Band bending increases with increasing ZnO doping, which reduces the tunneling barrier and the ρ_c. Figs. 4(b) and 4(c) quantitatively show the dependence of the contact resistivity on ZnO (IL) thickness and doping. More specifically, three cases arise when comparing the depletion width to the IL thickness. For the first case where the IL thickness is much smaller (<5 Å) than the depletion width, varying the depletion width by varying the doping will not affect the contact resistivity. Varying the IL thickness, on the other hand, will vary the tunnel barrier thickness and hence change the contact resistivity significantly. In the second case, for an intermediate IL thickness (5–15 Å), which is still less than the depletion width, varying the IL thickness will vary the tunneling barrier width significantly, more so for higher dopings, leading to large changes in resistivity (Fig. 4(c)). At the same time, increasing doping for a fixed IL thickness can lead to increased band bending (higher electric field) leading to lower resistivity. In the third case when the IL thickness is larger than the depletion width, varying the IL thickness will not cause a significant change in the tunneling barrier width (inset of Figs. 4(b) and 4(c)), which is now determined by the thinner depletion width, and hence the resistivity is more or less independent of the IL thickness. It will depend on doping only in as much as it changes the depletion width. Hence, ρ_c saturates with increasing ZnO thickness and eventually becomes thickness independent. Thus, IL doping is also beneficial from a process window and process variation standpoint for large scale integration.

IV. EXPERIMENTAL VERIFICATION

MIS contact diodes comparing n^+-ZnO, TiO_2, Al_2O_3, and ITO (10% Sn) ILs were fabricated on n-Ge substrates with Ti top metal contacts to verify the Fermi-level unpinning and ρ_c trends shown in Figs. 2 and 3. ZnO and ITO films were deposited using RF sputter deposition whereas Al_2O_3 and TiO_2 films were formed by ambient oxidation of thin Ti and Al films. The n^+-ZnO film was formed by annealing the deposited ZnO layer with a Ti top contact to create Vo donors.[9,25] The thicknesses of various IL layers were measured using spectroscopic ellipsometry and verified in a few cases using Transmission Electron Microscopy (TEM). Fig. 5(a) shows a cross-section schematic of the MIS diodes along with a TEM image of a Ti/ZnO/n-Ge stack and Fig. 5(b) shows experimental current density-voltage (*J–V*) characteristics for Ti/n-Ge, Ti/Al_2O_3 (2 nm)/n-Ge, Ti/TiO_2 (3 nm)/n-Ge, Ti/n^+-ZnO (2 nm)/n-Ge, and Ti/ITO (2 nm)/n-Ge diodes. Presence of an IL leads to FL unpinning and increase in the reverse bias current density. Also, 2 nm n^+-ZnO and ITO give less tunneling resistance as compared to 3 nm TiO_2 and 2 nm Al_2O_3 in agreement with the trends seen in the simulation results shown in Fig. 3. Fig. 5(c) shows the

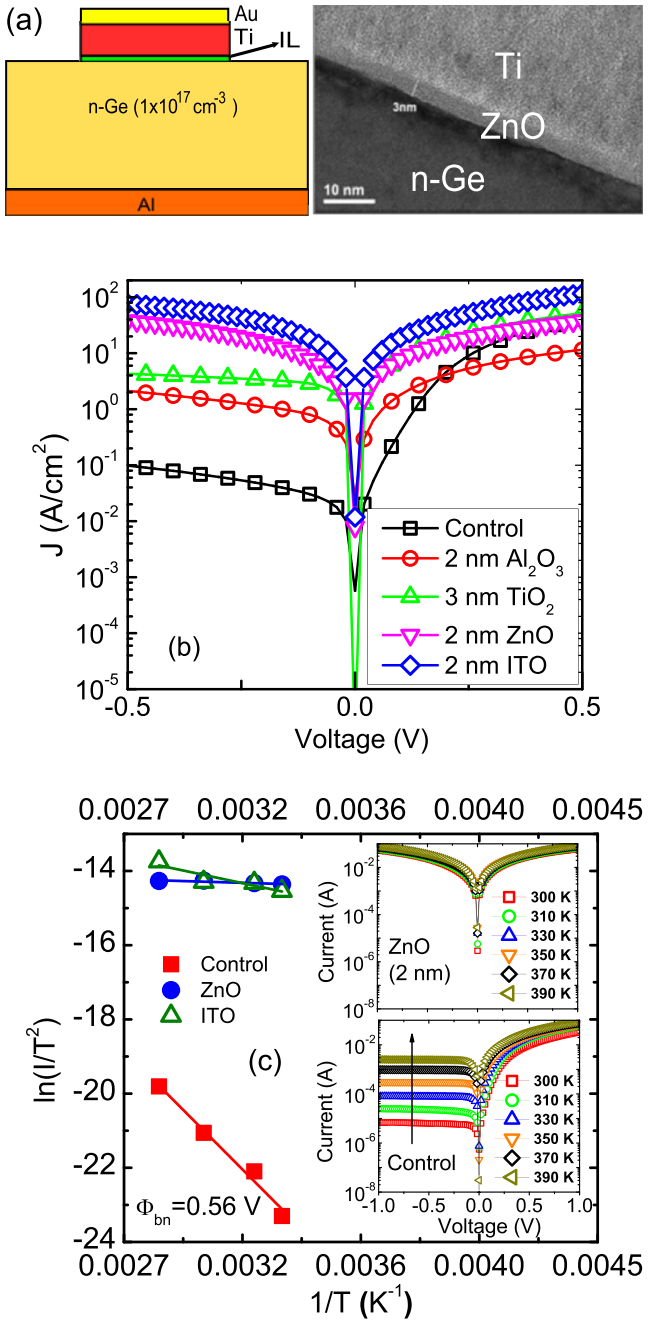

FIG. 5. (a) Cross-section schematic of fabricated MIS diodes on n-Ge along with a TEM image of a Ti/ZnO/n-Ge stack, (b) experimental verification of relative FL unpinning by different ILs as predicted by the MIGS model, and (c) temperature dependent *J–V* data for of Ti/n-Ge, Ti/ITO (2 nm)/n-Ge, and Ti/n^+-ZnO/n-Ge contacts.

temperature dependent *J–V* data for Ti/n^+-ZnO (2 nm)/n-Ge, Ti/ITO (2 nm)/n-Ge, and Ti/n-Ge diodes. Lower temperature dependence for the n^+-ZnO and ITO ILs indicates tunneling-dominated transport as opposed to the thermionic transport in control Ti/n-Ge diodes with a Schottky barrier height of nearly 0.56 V.

Further, to verify the lowering of contact resistance with n^+-ZnO IL on S/D-like heavy doped Ge layers, C-TLM (Circular-Transfer Length Method) structures using Ti/n^+-ZnO (1.5 nm)/n^+-Ge contacts were fabricated on epitaxially grown n^+-Ge with doping levels of 1×10^{19} and 2.5×10^{19} cm^{-3}. Fig. 6(a) shows a cross-section schematic

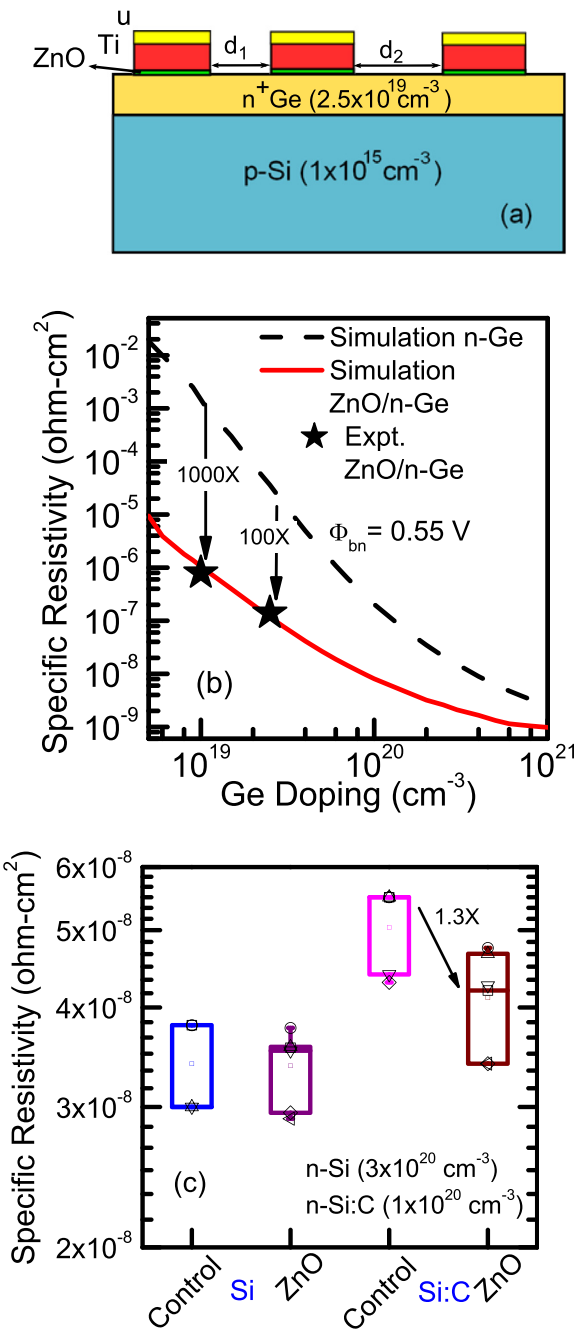

FIG. 6. (a) Cross-section schematic for fabricated circular TLM (C-TLM) Ti/n$^+$-ZnO/n-Ge structures on high doped n-Ge, (b) effect of substrate doping on the resistivity of ZnO/n-Ge MIS versus n-Ge M-S contacts, and (c) specific contact resistivity of Ti contacts on heavily doped epitaxial n-Si and n-Si:C layers with and without a ZnO IL as extracted from C-TLM measurements.

of the MIS C-TLM structures with an n$^+$-ZnO IL. As seen in Fig. 6(b), ρ_c is lower than Ti/n-Ge ρ_c ($\Phi_{bn} = 0.55$ V) by nearly 1000× at 1×10^{19} cm^{-3} and by 100× at 2.5×10^{19} cm^{-3} confirming the benefit seen with simulations (Fig. 3). Simulation setup described in Sec. II was used to fit the experimental data with ZnO doping as the fitting parameter. ZnO doping of 5×10^{19} cm^{-3} gave a reasonable fit. Fig. 6(b) shows that the advantage of MIS over M-S contact reduces with increasing substrate doping (dashed and solid lines converge). This is further illustrated in Fig. 6(c) which shows the specific contact resistivity extracted from C-TLM measurements on Ti contacts fabricated on epitaxial n-Si (3×10^{20} cm^{-3}) and n-Si:C (1×10^{20} cm^{-3}, 1.5% C) layers with and without a ZnO IL. While contact resistivity on the Si:C substrate decreases due to the ZnO IL, there is no change in contact resistivity with the ZnO IL for the more heavily doped Si substrate. In addition to Φ_{bn}, the thin depletion barrier due to high substrate doping also plays a role in determining the contact resistance.[26] Since most of the current transport is due to tunneling through the depletion barrier, the reduction in contact resistance due to a lower Φ_{bn} in a MIS contact is expected to be lower at high substrate dopings and should be a key metric for evaluation of MIS contacts. The diminishing benefit of MIS contacts at high substrate doping means that this scheme is more plausible for Ge/III-V substrates that suffer from low activated doping levels[27] or from surface depletion of dopants.

V. CONCLUSION

In summary, we have proposed a physics-based MIGS model for MIS contacts. Besides optimization of IL properties such as band offsets and thickness, doping of the IL is shown to give additional benefit in lowering MIS contact resistance. This is demonstrated through simulations of MIS contacts on n-Ge using ZnO and ITO ILs and experimentally verified through C-TLM and diode measurements on Ti/n$^+$-ZnO/n-Ge and Ti/ITO/n-Ge MIS contacts. While this work lays out a phenomenological framework for MIGS-based Fermi-level pinning in MIS contacts, a net additional dipole arising from O-ion density difference between the MIS interfaces and interfacial layers that can maximize this dipole effect, in addition to lowering MIGS, need to be considered in future studies on MIS contacts.

ACKNOWLEDGMENTS

The authors acknowledge the Department of Science and Technology, Government of India, for funding this work.

[1]C. O. Chui, H. Kim, P. McIntyre, and K. Saraswat, Tech. Dig. - Int. Electron Devices Meet. **2003**, 18.3.1–18.3.4.
[2]K. W. Ang, K. J. Chui, V. Bliznetsov, A. Du, N. Balasubramanian, M. F. Li, G. Samudra, and Y.-C. Yeo, Tech. Dig. - Electron Devices Meet. **2004**, 1069–1071.
[3]T. Nishimura, K. Kita, and A. Toriumi, Appl. Phys. Lett. **91**, 123123 (2007).
[4]A. Dimoulas, P. Tsipas, A. Sotiropoulos, and E. K. Evangelou, Appl. Phys. Lett. **89**, 252110 (2006).
[5]J. Kim, S. W. Bedell, S. L. Maurer, R. Loesing, and D. K. Sadana, Electrochem. Solid-State Lett. **13**, H12 (2010).
[6]V. P. Kishore, P. Paramahans, S. Sadana, U. Ganguly, and S. Lodha, Appl. Phys. Lett. **100**, 142107 (2012).
[7]M. Kobayashi, A. Kinoshita, K. Saraswat, H.-S. P. Wong, and Y. Nishi, J. Appl. Phys. **105**, 023702 (2009).
[8]D. Connelly, C. Faulkner, P. A. Clifton, and D. E. Grupp, Appl. Phys. Lett. **88**, 012105 (2006).
[9]P. Paramahans, R. K. Mishra, V. P. Kishore, P. Ray, A. Nainani, Y.-C. Huang, M. C. Abraham, U. Ganguly, and S. Lodha, Appl. Phys. Lett. **101**, 182105 (2012).
[10]A. Agrawal, N. Shukla, K. Ahmed, and S. Datta, Appl. Phys. Lett. **101**, 042108 (2012).
[11]A. Roy, J. Lin, and K. Saraswat, IEEE Electron Device Lett. **31**, 1077 (2010).
[12]W. Monch, Rep. Prog. Phys. **53**, 221 (1990).

[13]S. G. Louie, J. R. Chelikowsky, and M. L. Cohen, Phys. Rev. B **15**, 2154 (1977).
[14]J. F. Wager and J. Robertson, J. Appl. Phys. **109**, 094501 (2011).
[15]P. Paramahans, S. Gupta, R. K. Mishra, N. Agarwal, A. Nainani, Y. Huang, M. Abraham, S. Kapadia, U. Ganguly, and S. Lodha, Dig. Tech. Pap. – Symp. VLSI Technol. **2012**, 83–84.
[16]C. Tejedor, F. Flores, and E. Louis, J. Phys. C **10**, 2163 (1977).
[17]J. Tersoff, Phys. Rev. Lett. **52**, 465 (1984).
[18]Y.-C. Yeo, T.-J. King, and C. Hu, J. Appl. Phys. **92**, 7266 (2002).
[19]Z. Q. Liu, W. K. Chim, S. Y. Chiam, J. S. Pan, and C. M. Ng, J. Mater. Chem. **22**, 17887 (2012).
[20]J. Robertson and S. J. Clark, Phys. Rev. B **83**, 075205 (2011).
[21]W. A. Hadi, S. Chowdhury, M. S. Shur, and S. K. O'Leary, J. Appl. Phys. **112**, 123722 (2012).
[22]M. W. Allen and S. M. Durbin, Phys. Rev. B **82**, 165310 (2010).
[23]L. Lin, H. Li, and J. Robertson, Appl. Phys. Lett. **101**, 172907 (2012).
[24]W. Monch, J. Appl. Phys. **111**, 073706 (2012).
[25]H.-K. Kim, S.-H. Han, T.-Y. Seong, and W.-K. Choi, J. Electrochem. Soc. **148**, G114 (2001).
[26]K. Varahramyan and E. Verret, Solid-State Electron. **39**, 1601 (1996).
[27]C. O. Chui, K. Gopalakrishnan, P. B. Griffin, J. D. Plummer, and K. C. Saraswat, Appl. Phys. Lett. **83**, 3275 (2003).